The Astrophysical Journal Letters, 829:L10 (6pp), 2016 September 20 doi:10.3847/2041-8205/829/1/L10

CLUMPY AND EXTENDED STARBURSTS IN THE BRIGHTEST UNLENSED SUBMILLIMETER GALAXIES

Daisuke Iono[1,2], Min S. Yun[3], Itziar Aretxaga[4], Bunyo Hatsukade[1], David Hughes[4], Soh Ikarashi[5], Takuma Izumi[6], Ryohei Kawabe[1], Kotaro Kohno[6,7], Minju Lee[8], Yuichi Matsuda[1,2], Kouichiro Nakanishi[1,2], Toshiki Saito[8], Yoichi Tamura[6], Junko Ueda[9], Hideki Umehata[6], Grant Wilson[3], Tomonari Michiyama[2], and Misaki Ando[2]
[1] National Astronomical Observatory of Japan, National Institutes of Natural Sciences, 2-21-1 Osawa, Mitaka, Tokyo 181-8588, Japan; d.iono@nao.ac.jp
[2] SOKENDAI (The Graduate University for Advanced Studies), 2-21-1 Osawa, Mitaka, Tokyo 181-8588, Japan
[3] University of Massachusetts, Department of Astronomy, 710 North Pleasant Street, Amherst, MA 01003, USA
[4] Instituto Nacional de Astrofisica, Optica y Electronica (INAOE), Luis Enrique Erro 1, Sta. Ma. Tonantzintla, Puebla, Mexico
[5] Kapteyn Astronomical Institute, University of Groningen, P.O. Box 800, 9700AV Groningen, The Netherlands
[6] Institute of Astronomy, The University of Tokyo, 2-21-1 Osawa, Mitaka, Tokyo 181-0015, Japan
[7] Research Center for the Early universe, The University of Tokyo, 7-3-1 Hongo, Bunkyo, Tokyo 113-0033, Japan
[8] Department of Astronomy, The University of Tokyo, 7-3-1 Hongo, Bunkyo-ku, Tokyo 133-0033, Japan
[9] Harvard-Smithsonian Center for Astrophysics, 60 Garden Street, Cambridge, MA 02138, USA
Received 2016 July 18; revised 2016 September 3; accepted 2016 September 7; published 2016 September 19

ABSTRACT

The central structure in three of the brightest unlensed $z = 3$–4 submillimeter galaxies is investigated through 0.″015–0.″05 (120–360 pc) 860 μm continuum images obtained using the Atacama Large Millimeter/submillimeter Array (ALMA). The distribution in the central kiloparsec in AzTEC1 and AzTEC8 is extremely complex, and they are composed of multiple ∼200 pc clumps. AzTEC4 consists of two sources that are separated by ∼1.5 kpc, indicating a mid-stage merger. The peak star formation rate densities in the central clumps are ∼300–3000 $M_\odot\,\mathrm{yr}^{-1}\,\mathrm{kpc}^{-2}$, suggesting regions with extreme star formation near the Eddington limit. By comparing the flux obtained by ALMA and Submillimeter Array, we find that 68%–90% of the emission is extended ($\gtrsim$1 kpc) in AzTEC4 and 8. For AzTEC1, we identify at least 11 additional compact (∼200 pc) clumps in the extended 3–4 kpc region. Overall, the data presented here suggest that the luminosity surface densities observed at $\lesssim$150 pc scales are roughly similar to that observed in local ULIRGs, as in the eastern nucleus of Arp 220. Between 10% and 30% of the 860 μm continuum is concentrated in clumpy structures in the central kiloparsec, while the remaining flux is distributed over $\gtrsim$1 kpc regions, some of which could also be clumpy. These sources can be explained by a rapid inflow of gas such as a merger of gas-rich galaxies, surrounded by extended and clumpy starbursts. However, the cold mode accretion model is not ruled out.

Key words: galaxies: evolution – galaxies: formation – galaxies: high-redshift – galaxies: starburst

1. INTRODUCTION

Dusty star-forming galaxies (or submillimeter galaxies; SMGs) represent a population of the most massive young galaxies rapidly building up their mass in the early universe (Casey et al. 2014). The number density of the brightest SMGs with apparent submillimeter flux in excess of 10 mJy at 850 μm is ∼5 deg^{-2} (Hatsukade et al. 2016), and the intrinsic star formation rate (SFR) can exceed 1000 $M_\odot\,\mathrm{yr}^{-1}$ if the submillimeter flux arises entirely from star formation. Although they are rare, these SMGs host the most intense starbursts in the entire universe and may represent the formation sites of massive elliptical galaxies.

A merger of two gas-rich, massive spirals can account for the origin of the starburst galaxies with SFR ∼ 100 $M_\odot\,\mathrm{yr}^{-1}$. However, SMGs with SFR in excess of 1000 $M_\odot\,\mathrm{yr}^{-1}$ are difficult to explain with the conventional major merger scenario alone. Whether they are fueled and sustained through continuous accretion of cold gas (e.g., Kereš et al. 2005) and forming stars in wide-spread clumpy gas-rich disks (e.g., Bournaud et al. 2014), through gas-rich major mergers (e.g., Hayward et al. 2012; Miettinen et al. 2015) or through continuous infall of gas ejected via stellar feedback (Narayanan et al. 2015), understanding the physical origin of the intense star formation activity can only be achieved by high-resolution observations of the dust and gas.

The size scale and the spatial distribution of the submillimeter continuum in the bright SMGs are currently being studied using the Atacama Large Millimeter/submillimeter Array (ALMA). The sizes of the SMGs with $L_{\mathrm{IR}} \sim 10^{12-13}\,L_\odot$ have been constrained to 1.6–2.4 kpc from 0.″1–0.″7 observations (Ikarashi et al. 2015; Simpson et al. 2015; Oteo et al. 2016a), and the compactness suggests that they may become the compact quiescent galaxies found at $z \sim 2$ (Toft et al. 2014). The extended baseline capabilities of ALMA are now providing images at <0.″05 resolution (ALMA Partnership et al. 2015), allowing us to directly probe the central kiloparsec of these SMGs. Here, we present 0.″015–0.″05 resolution ALMA images in three of the brightest unlensed $z = 3$–4 SMGs in the COSMOS field—AzTEC1, AzTEC4, and AzTEC8. These sources were previously confirmed to be compact from 0.″5 images obtained at the Submillimeter Array (SMA; Ho et al. 2004; Younger et al. 2008, 2010) with no significant evidence of lensing by a foreground galaxy. All three sources were first discovered in the COSMOS field (Scoville et al. 2007) using the AzTEC camera mounted on the *James Clerk Maxwell Telescope* (Scott et al. 2008).

AzTEC1 has an SFR of 1300 $M_\odot\,\mathrm{yr}^{-1}$, dust mass of $(3.7 \pm 0.7) \times 10^{11}\,M_\odot$ assuming $T_d = 35$ K, and a stellar mass of $\sim 10^{11}\,M_\odot$ (Smolčić et al. 2011; Yun et al. 2015). The redshift of AzTEC1 is spectroscopically confirmed at $z = 4.3420 \pm 0.0004$ (Yun et al. 2015). AzTEC4 has a tentative hard X-ray source (Younger et al. 2010) and a *B*-band/*i*-band counterpart located ∼0.″5 away. The photometric redshift is $z \sim 4$ (Smolčić et al. 2011; Toft et al. 2014). A fit to

the SED yields an SFR of $1778\,M_{\odot}\,\mathrm{yr}^{-1}$, dust mass of $4.0\times10^{9}\,M_{\odot}$, IR luminosity of $1.7\times10^{13}\,L_{\odot}$, and a stellar mass of $1.6\times10^{11}\,M_{\odot}$ (Toft et al. 2014). In contrast to AzTEC4, AzTEC8 does not have a significant X-ray counterpart, but has a bright and extended VLA 20 cm emission to the east. The spectroscopic redshift of this source is $z=3.179$ (Smolčić et al. 2012), while the nearby radio source has a CO redshift of $z=1.950$ (M. Yun et al. 2016, in preparation). A fit to the SED yields an SFR of $2818\,M_{\odot}\,\mathrm{yr}^{-1}$, dust mass of $5.0\times10^{9}\,M_{\odot}$, IR luminosity of $2.8\times10^{13}\,L_{\odot}$, and a stellar mass of $3.2\times10^{11}\,M_{\odot}$ (Toft et al. 2014).

We adopt the *WMAP* concordance ΛCDM cosmology parameters with $H_0=69.6\,\mathrm{km\,s^{-1}\,Mpc^{-1}}$ and $\Omega_M=0.286$ (Bennett et al. 2014).

2. ALMA OBSERVATIONS

Observations were carried out on 2015 November 6–8, using 46–47 antennas with projected baselines that ranged from 100 m to 14 km. The manually calibrated data products were inspected in the visibilities and in the dirty image, and we flagged problematic antennas that were causing ripples in the image. We used CASA v4.5.1 for imaging. We placed CLEAN boxes to the regions where clear ($\geqslant3\sigma$) emission features are seen and CLEANed down to 1.5σ in order to properly image the extended emission. We searched for the optimal beam size by varying the Robust weighting. We tapered the AzTEC4 data to $0\farcs05$ since the emission is only marginally detected with the native resolution. The continuum image was generated by using all of the bands except for AzTEC1 in which the frequency range of the redshifted [C II] emission was excluded. For AzTEC1 and AzTEC8, we searched for the [C II] and [N II] emission by constructing images with $100\,\mathrm{km\,s^{-1}}$ resolution with a $0\farcs06$ beam. Both lines were undetected with 3σ upper limits of 1.4 mJy for AzTEC1 and 1.0 mJy for AzTEC8. The center frequency of the four correlator basebands was 350.739 GHz (855.337 μm).

An astrometry check source (J0930+0034) was observed several times within the main observing sequence. The emission peak of J0930+0034 in all data sets was found within $0\farcs0015$–$0\farcs0045$ of the phase center, and we adopt this value as the astrometric accuracy. We note that the peaks of all three sources were detected $\sim0\farcs05$ to $0\farcs4$ west of the phase center defined from the SMA position. The cause of this offset is unknown at present.

For AzTEC1, we obtained the $0\farcs3$ resolution data from the ALMA Archive (2012.1.00978.S) and combined it with our high-resolution data. The $0\farcs3$ resolution image alone is marginally resolved, with a total flux of 15.4 mJy. The center frequency was 343.769 GHz (872.679 μm), which is 7 GHz lower than the adopted frequency for the high-resolution data. Therefore, it is not tuned to the frequency of the redshifted [C II] line. Data combination was performed after down-weighting the $0\farcs3$ resolution data by 1/10, yielding a synthesized beam with reasonable sidelobe levels. The combined visibilities were then imaged using the multiscale CLEAN option in CASA, first without any visibility tapering, and then by varying the *outertaper* parameter from $0\farcs03$ to $0\farcs05$. The observed properties are presented in Table 1.

3. CHARACTERISTICS OF THE INDIVIDUAL SOURCES

The ALMA images and the derived parameters are presented in Figures 1–2 and Table 2. We derive the SFR of each component by scaling the total SFR with the ratio between the derived flux densities and the total SMA flux. The luminosity ($\Sigma_{\mathrm{L_{FIR}}}$) and SFR surface densities (Σ_{SFR}) are derived by using the observed source size measurements presented in Table 2. The peak brightness temperatures using the optically thick Planck equation are 33–82 K.

AzTEC1—From the $0\farcs026\times0\farcs018$ resolution image (Figure 1(a)), we find that the central $\lesssim$0.5 kpc region of AzTEC1 is characterized by two central peaks, each with $249\pm31\,\mu\mathrm{Jy\,beam^{-1}}$ and $227\pm31\,\mu\mathrm{Jy\,beam^{-1}}$ and a separation of ∼150 pc. The double-peak structure is surrounded by a complex emission that extends to $\lesssim$0.5 kpc scale, and the total flux enclosed within the red 3σ contours is 1.54 ± 0.15 mJy.

The >0.5 kpc region of AzTEC1 is characterized by two distinct features: (1) smooth and extended emission that reaches 3–4 kpc to the north (see Figure 2(c)), and (2) numerous ∼200 pc scale clumps found in the extended region (see Figure 2(a)). The excellent consistency between the total flux in the $0\farcs070\times0\farcs063$ image in Figure 2(c) (14.16 ± 1.42 mJy) and the SMA image (13.8 ± 2.3 mJy) suggests that much of the extended features are real. In order to quantify the size of the emission in the central kiloparsec and the associated flux, the peak emission of Figure 2(c) was modeled with a two-dimensional Gaussian. We obtain $(0\farcs102\pm0\farcs007)\times(0\farcs083\pm0\farcs006)$, which is equivalent to $(700\pm50)\times(570\pm40)$ pc, with an integrated flux density of 4.52 ± 0.23 mJy (32% of the total flux). This suggests that the extended structure contains 68% (9.64 ± 1.44 mJy) of the total flux. The half-light radius is 1.1 ± 0.1 kpc.

In the >0.5 kpc region, we have manually identified ∼40 compact clumps that are detected at 3σ or above. The number reduces to 11 clumps if we set the threshold to 4σ. The number of negative 3σ and 4σ clumps in the same region are two and one, respectively. The source sizes, integrated flux densities, SFR, and the Σ_{SFR} are summarized in Table 3. The average source size is $(0.30\pm0.05)\times(0.17\pm0.03)$ kpc, and the total flux from all of the $\geqslant4\sigma$ clumps is 2.69 ± 0.27 mJy, which translates to an SFR of $250\pm30\,M_{\odot}\,\mathrm{yr}^{-1}$.

AzTEC4—At $0\farcs05$ resolution, the emission in AzTEC4 is divided into two distinct clumps with a separation of ∼1.5 kpc in the north–south direction. The large separation between the two clumps suggests that AzTEC4 is a mid-stage merger. The peaks of the northern and southern sources are $536\pm61\,\mu\mathrm{Jy\,beam^{-1}}$ and $435\pm61\,\mu\mathrm{Jy\,beam^{-1}}$, and the deconvolved source sizes from a two-dimensional Gaussian fit are $(0\farcs130\pm0\farcs023)\times(0\farcs086\pm0\farcs017)$ and $(0\farcs132\pm0\farcs030)\times(0\farcs056\pm0\farcs018)$, respectively. We have further inspected the residuals after subtracting both sources from the image and found that the image is dominated by noise. The total integrated flux of the northern and southern sources are 1.98 ± 0.31 mJy and 1.28 ± 0.25 mJy, respectively, yielding a total of 3.26 ± 0.40 mJy. The total flux derived from the $0\farcs86\times0\farcs77$ SMA beam is 13.1 ± 1.8 mJy for a Gaussian model (Younger et al. 2010). Therefore, 75% of the total flux is missing in the extended structure.

AzTEC8—The central region is clearly resolved into two clumps separated by ∼200 pc in the east–west direction. The peak of the eastern and western clumps are $273\pm34\,\mu\mathrm{Jy\,beam^{-1}}$ and $296\pm34\,\mu\mathrm{Jy\,beam^{-1}}$, respectively.

Table 1
Observational Properties

Source	Redshift	1 arcsec (kpc)	R.A. (J2000)	Decl. (J2000)	rms (μJy)	beam (Position Angle)	Robust[a]	S_{860}[b] (mJy)
AzTEC1	4.342	6.7	9:59:42.86	+2:29:38.2	31	0.″026 × 0.″018 (46°)	2	3.67 ± 0.37
					38	0.″048 × 0.″039 (42°)	2 (0.″03)	9.09 ± 0.91
					56	0.″070 × 0.″063 (41°)	2 (0.″05)	14.16 ± 1.42
AzTEC4	~4[c]	7.1	9:59:31.72	+2:30:44.0	61	0.″064 × 0.″057 (40°)	2 (0.″05)	3.26 ± 0.40
AzTEC8	3.179	7.7	9:59:59.34	+2:34:41.0	34	0.″017 × 0.″014 (87°)	0.5	1.63 ± 0.16

Notes.
[a] The value of Robust parameter used in CASA. The values in parentheses are used for the *outertaper* in the CASA task CLEAN.
[b] Total ALMA flux above 3σ. For AzTEC1, we integrate the $\geqslant 3\sigma$ emission in Figure 2. The SMA 880 μm fluxes (beam sizes) are 13.8 ± 2.3 (0.″86 × 0.″55), 13.1 ± 1.8 (0.″86 × 0.″77), and 17.7 ± 2.3 mJy (0.″86 × 0.″55), for AzTEC1, AzTEC4, and AzTEC8, respectively (Younger et al. 2008, 2010).
[c] The photometric redshifts derived in the literature are $4.70^{+0.43}_{-1.11}$ (Younger et al. 2007) and $4.93^{+0.43}_{-1.11}$ (Smolčić et al. 2012; Toft et al. 2014). We adopt $z = 4$ for all calculations in this Letter.

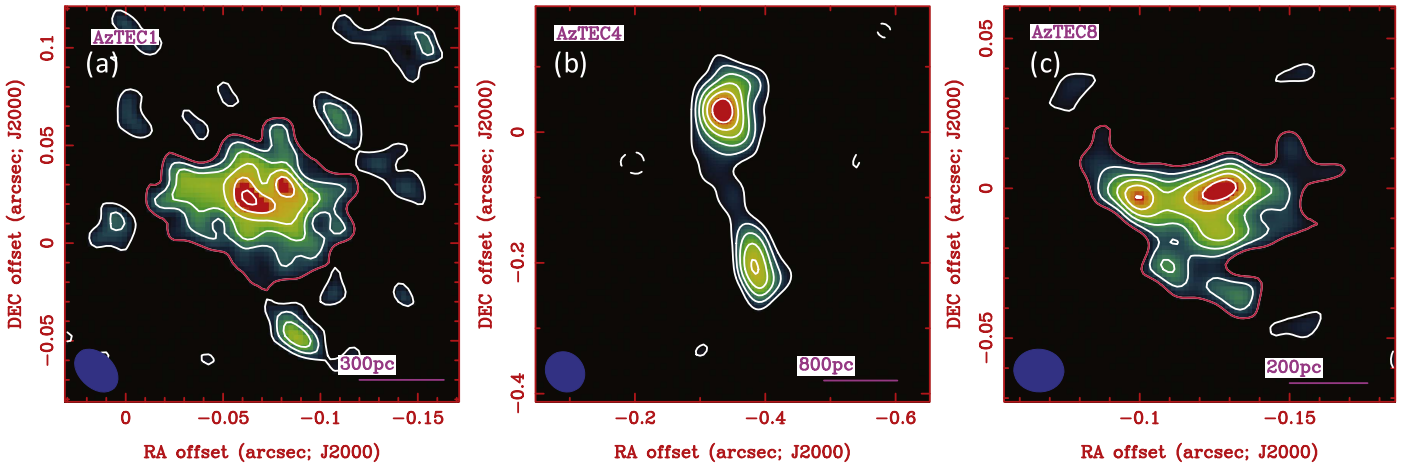

Figure 1. 860 μm images of (a) AzTEC1 (Robust = 2 and no tapering), (b) AzTEC4 (Robust = 2 and *outertaper* = 0.″05), and (c) AzTEC8 (Robust = 0.5). The physical scale shown in the lower right corner of each panel assumes $z = 4.342$ for AzTEC1, $z = 4$ for AzTEC4, and $z = 3.179$ for AzTEC8. The lowest contours represent 3σ, and they increase in steps of 1σ (the 1σ values are shown in Table 1). Negative contours are shown as dashed lines. The total flux enclosed within the red 3σ contour for AzTEC1 and 8 are used to derive the parameters in Table 2. All of the images are referenced from the SMA coordinates.

The total integrated flux in the central kiloparsec (region within the red contour in Figure 1) is 1.63 ± 0.16 mJy. The total flux derived from the 0.″86 × 0.″55 SMA beam is 17.7 ± 2.3 mJy for a Gaussian model (Younger et al. 2010), and thus ~90% of the flux is in the extended structure.

4. NATURE OF THE CENTRAL STAR-FORMING REGION

4.1. Eddington Limited Starbursts?

The stellar radiation pressure imposed upon the surrounding optically thick dust and gas can provide an important stabilization mechanism for gas against self-gravity. Assuming a one-zone moderately optically thick disk model, a Toomre-stable ($Q \sim 1$) disk, and $T < 100$ K, the $\Sigma_{\rm SFR}$ required to support the disk with radiation pressure is $\sim 1000\,M_\odot\,{\rm yr}^{-1}\,{\rm kpc}^{-2}$ (Thompson et al. 2005). At higher temperatures (T = 100–200 K), which may be more appropriate at the centers of ULIRGs (Wilson et al. 2014) and SMGs, the correlation between opacity and temperature breaks down, and $\Sigma_{\rm SFR}$ becomes a function of various model parameters such as rotation velocity, gas mass fraction, and opacity. We lack sufficient data, such as gas kinematics, to constrain these parameters properly, and the required $\Sigma_{\rm SFR}$ can be $\sim$100–2000 $M_\odot\,{\rm yr}^{-1}\,{\rm kpc}^{-2}$ (see Equation (28) of Thompson et al. 2005) even with a conservative set of assumptions.

The integrated and beam-averaged peak $\Sigma_{\rm SFR}$ ranges from 280 ± 130 to $960 \pm 240\,M_\odot\,{\rm yr}^{-1}\,{\rm kpc}^{-2}$ for AzTEC1 and AzTEC4. On the other hand, the $\Sigma_{\rm SFR}$ of the entire AzTEC1 is much lower ($130 \pm 30\,M_\odot\,{\rm yr}^{-1}\,{\rm kpc}^{-2}$), and it is close to the lower end of the predicted $\Sigma_{\rm SFR}$ for a radiation pressure supported disk. These are consistent with the average $\Sigma_{\rm SFR}$ found in the most luminous starburst galaxies observed in the early universe (80–1000 $M_\odot\,{\rm yr}^{-1}\,{\rm kpc}^{-2}$; Tacconi et al. 2006; Walter et al. 2009; Riechers et al. 2013, 2014; Hodge et al. 2015; Oteo et al. 2016a, 2016b). The gravitationally lensed source SDP.81 (SFR ~ 500 $M_\odot\,{\rm yr}^{-1}$) was observed at 200 pc resolution (ALMA Partnership et al. 2015), and the $\Sigma_{\rm SFR}$ of the 14 clumps range from ~100 to 400 $M_\odot\,{\rm yr}^{-1}\,{\rm kpc}^{-2}$ (Hatsukade et al. 2015), which is slightly lower than the central regions of AzTEC1 and AzTEC8. In contrast to AzTEC1 and AzTEC4, the average $\Sigma_{\rm SFR}$ in AzTEC8 is close to the upper end of the model predictions. The beam-averaged peak values are even higher (~3000 $M_\odot\,{\rm yr}^{-1}\,{\rm kpc}^{-2}$). The extreme values derived in AzTEC8 may suggest that it is forming stars near or above the Eddington limit.

4.2. Comparison with Local U/LIRGs

The nearby late-stage merging ULIRG Arp 220 was recently observed using ALMA at 0.″36 × 0.″20 (Wilson et al. 2014)

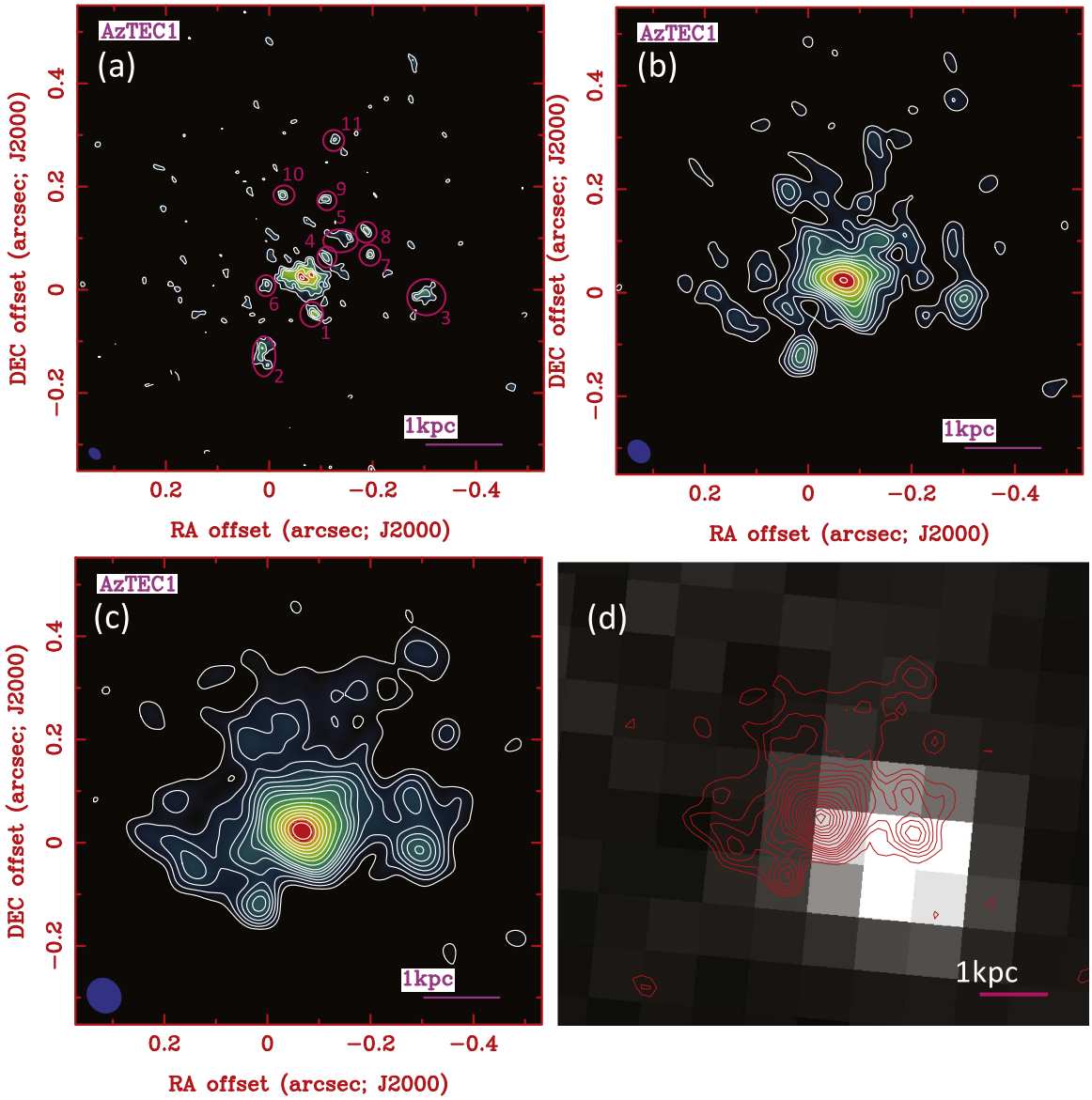

Figure 2. 860 μm images of AzTEC1 with (a) $0\farcs026 \times 0\farcs018$, (b) $0\farcs048 \times 0\farcs039$, and (c) $0\farcs070 \times 0\farcs063$ resolution. The lowest contours represent 3σ, and they increase in steps of 1σ up to 10σ and steps of 2σ beyond. The properties of the clumps labeled 1–11 in (a) are presented in Table 3. (d) Overlay of ALMA contours on the *HST* F160W image. The contour levels are the same as in (c). We note a $\sim 0\farcs2$ offset between the ALMA peak and the *HST* peak (see also Olivares et al. 2016). Detailed investigation of the relative astrometry is deferred to a future analysis.

and $0\farcs32 \times 0\farcs28$ (Scoville et al. 2015) resolution at 690 GHz. Assuming $1'' = 475$ pc, these correspond to 100–170 pc scales, allowing us a direct comparison with the physical properties of AzTEC1 and AzTEC8. The luminosity surface densities in Arp 220 are $\geqslant 10^{14}$ $L_\odot$ kpc^{-2} and 10^{12-13} $L_\odot$ kpc^{-2} for the western and eastern nucleus, respectively (Wilson et al. 2014; see also Downes & Eckart 2007; Sakamoto et al. 2008; Barcos-Muñoz et al. 2015). The average luminosity densities derived in the central peaks of AzTEC1 [$(7.8 \pm 2.3) \times 10^{12}$ $L_\odot$ kpc^{-2}] and AzTEC8 [$(2.8 \pm 0.6) \times 10^{13}$ $L_\odot$ kpc^{-2}] are consistent with the eastern nucleus, but an order of magnitude lower than the western nucleus of Arp220. The high value in the western nucleus may be attributed to the presence of an AGN. In contrast, the same quantities derived in the less luminous mid-stage merging LIRG VV114 is at least 2–3 orders of magnitude lower (Saito et al. 2015).

5. DISCUSSION AND SUMMARY

5.1. Nature of the Clumpy and Extended Emission in AzTEC1

The important new finding from the AzTEC1 map is the presence of compact (~200 pc) clumps and the diffuse and extended emission out to 3–4 kpc.

Compact Clumps—These clumps can grow to contain a stellar mass of $\sim 10^9$ $M_\odot$ by $z = 2$ (2 Gyr), even if they are converting gas to stars at an efficiency of 10% (Larson 1982). Numerical simulations of isolated gas-rich disks suggest that gas clumps of $\sim 10^9$ $M_\odot$ survive for at least 10^8 years during the course of their lifetime (Bournaud et al. 2014). These massive clumps can migrate inwards via dynamical friction and coalesce with the central galaxy within a Gyr timescale (Noguchi 1999; Hopkins et al. 2012; Inoue & Saitoh 2012). We note that the sizes and ubiquity of the clumps are similar to the young super star clusters found in the central region of

Table 2
Star Formation Properties in the Central Kiloparsec

Source	Component	S_{860} (mJy)	Size (kpc^2)	$L_{\rm FIR}$ ($L_\odot$)	$\Sigma_{L_{\rm FIR}}$ ($L_\odot$ kpc^{-2})	SFR ($M_\odot$ yr^{-1})	$\Sigma_{\rm SFR}$ ($M_\odot$ yr^{-1} kpc^{-2})
AzTEC1	Total[a]	14.16 ± 1.42	10.15 ± 1.62	1.1×10^{13}	$(1.1 \pm 0.2) \times 10^{12}$	1300	130 ± 30
	Integrated[b]	1.54 ± 0.15	0.27 ± 0.04	$(1.2 \pm 0.2) \times 10^{12}$	$(4.6 \pm 3.0) \times 10^{12}$	150 ± 40	540 ± 160
	Central Peak	0.25 ± 0.03	⋯	$(2.0 \pm 0.4) \times 10^{11}$	$(8.1 \pm 1.7) \times 10^{12}$	23 ± 6	960 ± 240
	Western Peak	0.23 ± 0.03	⋯	$(1.8 \pm 0.4) \times 10^{11}$	$(7.4 \pm 1.6) \times 10^{12}$	21 ± 5	870 ± 220
AzTEC4[c]	Total[d]	13.1 ± 1.8	⋯	1.7×10^{13}	⋯	1778 ± 733	⋯
	Northern Source	1.98 ± 0.31	0.64 ± 0.17	$(2.6 \pm 0.5) \times 10^{12}$	$(4.0 \pm 1.9) \times 10^{12}$	270 ± 120	420 ± 220
	Southern Source	1.28 ± 0.25	0.42 ± 0.17	$(1.7 \pm 0.4) \times 10^{12}$	$(3.7 \pm 3.5) \times 10^{12}$	170 ± 80	410 ± 250
	North+South	3.26 ± 0.40	1.06 ± 0.24	$(4.2 \pm 0.8) \times 10^{12}$	$(4.0 \pm 1.1) \times 10^{12}$	440 ± 200	420 ± 210
	Northern Peak	0.54 ± 0.06	⋯	$(7.0 \pm 1.2) \times 10^{11}$	$(3.3 \pm 0.6) \times 10^{12}$	73 ± 33	350 ± 160
	Southern Peak	0.44 ± 0.06	⋯	$(5.6 \pm 1.1) \times 10^{11}$	$(2.7 \pm 0.5) \times 10^{12}$	59 ± 27	280 ± 130
AzTEC8[c]	Total[d]	17.7 ± 2.3	⋯	2.8×10^{13}	⋯	2818 ± 66	⋯
	Integrated[b]	1.63 ± 0.16	0.16 ± 0.02	$(2.6 \pm 0.4) \times 10^{12}$	$(1.6 \pm 1.3) \times 10^{13}$	260 ± 40	1620 ± 330
	Western Peak	0.30 ± 0.03	⋯	$(4.7 \pm 0.6) \times 10^{11}$	$(2.9 \pm 0.4) \times 10^{13}$	47 ± 8	2950 ± 520
	Eastern Peak	0.27 ± 0.03	⋯	$(4.3 \pm 0.6) \times 10^{11}$	$(2.7 \pm 0.4) \times 10^{13}$	43 ± 8	2720 ± 490

Notes.
[a] Using the size of the region enclosed within the 3σ contours in Figure 2(c). The IR luminosity and SFR are obtained from Yun et al. (2015).
[b] Using the total ALMA flux in the region enclosed within the red 3σ contour in Figure 1.
[c] The IR luminosity and SFR are obtained from Toft et al. (2014).
[d] Using the SMA flux.

Table 3
Sizes and Star Formation Properties of Clumps in AzTEC1

ID	Source Size (arcsec)	Source Size (kpc)	Flux Density (mJy)	SFR ($M_\odot$ yr^{-1})	$\Sigma_{\rm SFR}$ ($M_\odot$ yr^{-1} kpc^{-2})
1	(0.″036 ± 0.″008) × (0.″021 ± 0.″003)	(0.25 ± 0.06) × (0.14 ± 0.02)	0.283 ± 0.079	27 ± 9	650 ± 280
2	(0.″055 ± 0.″014) × (0.″028 ± 0.″005)	(0.38 ± 0.09) × (0.19 ± 0.03)	0.486 ± 0.130	46 ± 14	560 ± 240
3	(0.″048 ± 0.″013) × (0.″029 ± 0.″006)	(0.33 ± 0.09) × (0.20 ± 0.04)	0.432 ± 0.127	41 ± 14	530 ± 250
4	(0.″042 ± 0.″012) × (0.″021 ± 0.″004)	(0.29 ± 0.08) × (0.15 ± 0.03)	0.275 ± 0.090	26 ± 10	530 ± 270
5	(0.″041 ± 0.″013) × (0.″023 ± 0.″005)	(0.28 ± 0.09) × (0.16 ± 0.03)	0.264 ± 0.094	25 ± 10	490 ± 260
6	(0.″034 ± 0.″010) × (0.″028 ± 0.″007)	(0.23 ± 0.07) × (0.20 ± 0.05)	0.268 ± 0.099	25 ± 10	490 ± 270
7	<0.″026 × <0.″018	<0.18 × <0.12	0.136 ± 0.031	13 ± 4	>500
8	<0.″026 × <0.″018	<0.18 × <0.12	0.143 ± 0.029	13 ± 4	>500
9	<0.″026 × <0.″018	<0.18 × <0.12	0.138 ± 0.032	13 ± 4	>500
10	<0.″026 × <0.″018	<0.18 × <0.12	0.143 ± 0.032	13 ± 4	>500
11	<0.″026 × <0.″018	<0.18 × <0.12	0.122 ± 0.034	11 ± 4	>500
Mean[a]	(0.″043 ± 0.″008) × (0.″025 ± 0.″004)	(0.30 ± 0.05) × (0.17 ± 0.03)	0.335 ± 0.098	32 ± 9	540 ± 60

Note.
[a] Mean and standard deviation of the sources that are resolved (i.e., ID = 1–6).

Arp 220 (Scoville et al. 1998; Shioya et al. 2001; Wilson et al. 2006).

Diffuse Extended Emission—The extended emission accounts for 68% (SFR = 880 ± 130 $M_\odot$ yr^{-1}) of the total flux. This is consistent with the finding by Yun et al. (2015), whose SED modeling required ∼50% of the gas and dust to be outside the central kiloparsec in order to account for the rest-frame optical light. The extended structure may suggest a presence of a 3–4 kpc starbursting disk or a massive starburst-driven outflow from the central kiloparsec. Alternatively, the extended material can quickly cool and settle into a compact star-forming disk.

5.2. Emerging Picture

The new ALMA data presented here suggest that the central region of some of the brightest unlensed SMGs in the universe (AzTEC1 and AzTEC8) are very compact ($\leqslant$0.5 kpc) and contain at least two central clumps, forming stars near the Eddington limit, with physical properties that are similar to the eastern nucleus of Arp220. AzTEC4 consists of two sources that are separated by ∼1.5 kpc, indicating a mid-stage merger. In addition, we find that 68%–90% of the emission is distributed over $\gtrsim$1 kpc regions in all three sources.

A major merger of two gas-rich galaxies can explain the morphology and the physical properties seen in the central kiloparsec of all three AzTEC sources. However, this scenario alone cannot explain the large amount of extended emission. The extended structure with numerous clumps (particularly for AzTEC1) is reminiscent of an isolated clumpy star-forming disk model which is often invoked to explain the morphology and kinematics of high-redshift star-forming galaxies (e.g., Förster Schreiber et al. 2009; Bournaud et al. 2014). However, the characteristic sizes of these disks are a factor of 2–3 larger than the sizes of the AzTEC sources ($\lesssim$3–4 kpc). Although the sample size used in this study is small, we suggest a hybrid scenario, i.e., a merging central ULIRG surrounded by clumpy and extended starbursting material, to be the favorable model

here. The relative compactness of these sources supports the idea that these SMGs will become the compact massive galaxies found at $z \sim 2$ (e.g., Hayward et al. 2012; Toft et al. 2014; Ikarashi et al. 2015; Simpson et al. 2015; van Dokkum et al. 2015; Wellons et al. 2015). Alternatively, the extended material can quickly reform a disk, becoming a bulge-dominated disk galaxy (Springel & Hernquist 2005; Hopkins et al. 2009; Ueda et al. 2014). Detailed kinematical information of gas will provide us with better insight of the overall picture.

We thank our referee for valuable comments that improved the contents of this Letter significantly. We thank P. Cox, S. Iguchi, T. Kodama, D. Narayanan, and J. Simpson for useful discussion. D.I. is supported by Japan Society for Promotion of Science (JSPS) KAKENHI (No. 15H02074) and by the 2015 Inamori Research Grants Program. This work was performed in part at the Aspen Center for Physics, which is supported by National Science Foundation grant PHY-1066293. S.I. acknowledges the support of the Netherlands Organization for Scientific Research (NWO) through the Top Grant Project 614.001.403. This Letter makes use of the following ALMA data: ADS/JAO. ALMA#2012.1.00978.S and #2015.1.01345.S. ALMA is a partnership of ESO (representing its member states), NSF (USA) and NINS (Japan), together with NRC (Canada), NSC and ASIAA (Taiwan), and KASI (Republic of Korea), in cooperation with the Republic of Chile. The Joint ALMA Observatory is operated by ESO, AUI/NRAO and NAOJ.

REFERENCES

ALMA Partnership, Vlahakis, C., Hunter, T. R., et al. 2015, ApJL, 808, L4
Barcos-Muñoz, L., Leroy, A. K., Evans, A. S., et al. 2015, ApJ, 799, 10
Bennett, C. L., Larson, D., Weiland, J. L., & Hinshaw, G. 2014, ApJ, 794, 135
Bournaud, F., Perret, V., Renaud, F., et al. 2014, ApJ, 780, 57
Casey, C. M., Narayanan, D., & Cooray, A. 2014, PhR, 541, 45
Downes, D., & Eckart, A. 2007, A&A, 468, L57
Förster Schreiber, N. M., Genzel, R., Bouché, N., et al. 2009, ApJ, 706, 1364
Hatsukade, B., Kohno, K., Umehata, H., et al. 2016, PASJ, 68, 36
Hatsukade, B., Tamura, Y., Iono, D., et al. 2015, PASJ, 67, 93
Hayward, C. C., Jonsson, P., Kereš, D., et al. 2012, MNRAS, 424, 951
Ho, P. T. P., Moran, J. M., & Lo, K. Y. 2004, ApJL, 616, L1
Hodge, J. A., Riechers, D., Decarli, R., et al. 2015, ApJL, 798, L18
Hopkins, P. F., Cox, T. J., Younger, J. D., & Hernquist, L. 2009, ApJ, 691, 1168
Hopkins, P. F., Kereš, D., Murray, N., Quataert, E., & Hernquist, L. 2012, MNRAS, 427, 968
Ikarashi, S., Ivison, R. J., Caputi, K. I., et al. 2015, ApJ, 810, 133
Inoue, S., & Saitoh, T. R. 2012, MNRAS, 422, 1902
Kereš, D., Katz, N., Weinberg, D. H., & Davé, R. 2005, MNRAS, 363, 2
Larson, R. B. 1982, MNRAS, 200, 159
Miettinen, O., Novak, M., Smolčić, V., et al. 2015, A&A, 584, A32
Narayanan, D., Turk, M., Feldmann, R., et al. 2015, Natur, 525, 496
Noguchi, M. 1999, ApJ, 514, 77
Olivares, V., Treister, E., Privon, G. C., et al. 2016, ApJ, 827, 57
Oteo, I., Ivison, R. J., Dunne, L., et al. 2016a, ApJ, 827, 34
Oteo, I., Zwaan, M. A., Ivison, R. J., Smail, I., & Biggs, A. D. 2016b, arXiv:1607.06464
Riechers, D. A., Bradford, C. M., Clements, D. L., et al. 2013, Natur, 496, 329
Riechers, D. A., Carilli, C. L., Capak, P. L., et al. 2014, ApJ, 796, 84
Saito, T., Iono, D., Yun, M. S., et al. 2015, ApJ, 803, 60
Sakamoto, K., Wang, J., Wiedner, M. C., et al. 2008, ApJ, 684, 957
Scott, K. S., Austermann, J. E., Perera, T. A., et al. 2008, MNRAS, 385, 2225
Scoville, N., Abraham, R. G., Aussel, H., et al. 2007, ApJS, 172, 38
Scoville, N., Sheth, K., Walter, F., et al. 2015, ApJ, 800, 70
Scoville, N. Z., Evans, A. S., Dinshaw, N., et al. 1998, ApJL, 492, L107
Shioya, Y., Taniguchi, Y., & Trentham, N. 2001, MNRAS, 321, 11
Simpson, J. M., Smail, I., Swinbank, A. M., et al. 2015, ApJ, 799, 81
Smolčić, V., Aravena, M., Navarrete, F., et al. 2012, A&A, 548, A4
Smolčić, V., Capak, P., Ilbert, O., et al. 2011, ApJL, 731, L27
Springel, V., & Hernquist, L. 2005, ApJL, 622, L9
Tacconi, L. J., Neri, R., Chapman, S. C., et al. 2006, ApJ, 640, 228
Thompson, T. A., Quataert, E., & Murray, N. 2005, ApJ, 630, 167
Toft, S., Smolčić, V., Magnelli, B., et al. 2014, ApJ, 782, 68
Ueda, J., Iono, D., Yun, M. S., et al. 2014, ApJS, 214, 1
van Dokkum, P. G., Nelson, E. J., Franx, M., et al. 2015, ApJ, 813, 23
Walter, F., Riechers, D., Cox, P., et al. 2009, Natur, 457, 699
Wellons, S., Torrey, P., Ma, C.-P., et al. 2015, MNRAS, 449, 361
Wilson, C. D., Harris, W. E., Longden, R., & Scoville, N. Z. 2006, ApJ, 641, 763
Wilson, C. D., Rangwala, N., Glenn, J., et al. 2014, ApJL, 789, L36
Younger, J. D., Fazio, G. G., Ashby, M. L. N., et al. 2010, MNRAS, 407, 1268
Younger, J. D., Fazio, G. G., Huang, J.-S., et al. 2007, ApJ, 671, 1531
Younger, J. D., Fazio, G. G., Wilner, D. J., et al. 2008, ApJ, 688, 59
Yun, M. S., Aretxaga, I., Gurwell, M. A., et al. 2015, MNRAS, 454, 3485